

## Pumping of liquids with ac voltages applied to asymmetric pairs of microelectrodes

A. Ramos,<sup>1,\*</sup> A. González,<sup>2</sup> A. Castellanos,<sup>1</sup> N. G. Green,<sup>3</sup> and H. Morgan<sup>3</sup>

<sup>1</sup>*Departamento de Electrónica y Electromagnetismo, University of Seville, Avenida Reina Mercedes s/n, 41012 Sevilla, Spain*

<sup>2</sup>*Departamento de Física Aplicada, ESI University of Seville, Camino de los Descubrimientos s/n, 41092 Sevilla, Spain*

<sup>3</sup>*Department of Electronics and Electrical Engineering, University of Glasgow, Glasgow G12 8LT, Scotland, United Kingdom*

(Received 25 July 2002; revised manuscript received 13 February 2003; published 9 May 2003)

The net flow of electrolyte induced by an ac electric potential applied to an array of asymmetric pairs of microelectrodes has recently been reported. The interaction between the oscillating electric field and the oscillating induced charge at the diffuse double layer on the electrodes results in a steady electro-osmotic velocity distribution on top of the electrodes. This slip velocity distribution is anisotropic and produces a net flow of fluid. This paper presents a theoretical analysis of the pumping phenomena based upon an electro-osmotic model in ac fields. The electrical equations are solved numerically using the charge simulation method. The bulk flow generated by the electro-osmotic slip velocity is calculated. The dependence of the fluid flow on voltage and frequency is described and compared to experiments.

DOI: 10.1103/PhysRevE.67.056302

PACS number(s): 47.65.+a, 82.45.-h, 82.70.Dd, 85.85.+j

### I. INTRODUCTION

The last decade has seen a rapid growth in the development of integrated microanalytical devices that function as a laboratory on a chip [1]. New types of microelectromechanical systems [2] are also being developed. In both cases, there is a requirement for precise control of small masses of liquids, particularly where devices are used in the field of chemical and bioanalytical sciences [3]. Many techniques have been developed to pump liquids, including micromechanical methods [4], electro-osmosis [5], electrowetting [6], thermocapillary pumping [7], and electrohydrodynamic pumping [8]. However, there are inherent drawbacks to all of these systems; some require external temperature gradients or high applied voltages, others use moving parts or produce pulsating flow.

Recently, Brown *et al.* [9] have demonstrated pumping of an electrolyte on an array of asymmetric microelectrodes energized by a single ac signal of the order of kHz and at low voltage (around 1 V). The system is, therefore, of interest in the development of micropumps. This type of pump followed from the theoretical arguments regarding the unidirectional flow resulting from spatially asymmetric applied potentials [10]. The physical mechanism responsible for the flow is electro-osmosis in ac fields, where nonuniformities in the field geometry produce a nonzero time-averaged electro-osmotic slip velocity at the surface of the electrodes [11–14]. It should be noted that this type of fluid flow is distinct from flow originated from electrothermal effects [8,15] which are found at higher frequencies and generally, higher electrolyte conductivities.

The mechanism responsible for driving the flow is illustrated in Fig. 1(a), drawn for the geometry used by Brown *et al.* An alternating potential difference is applied to each pair of asymmetric electrodes creating a nonuniform electric field. At a certain time, the situation is as shown in the figure;

the component of the field normal to the electrode induces a charge in the diffuse double layer; the tangential component of the field produces a force on the induced charge. The force has a nonzero time average because if the sign of the field reverses, so does the sign of the charge. This force produces

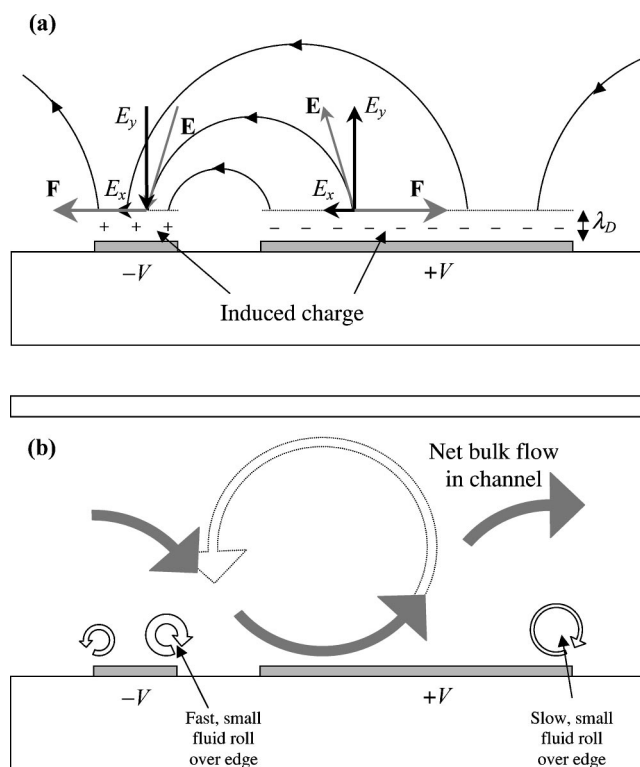


FIG. 1. Schematic diagram of the physical mechanism of ac electro-osmosis in an asymmetric electrode array inside a microfluidic channel. (a) A diagram showing the charge induced in response to applied potentials on the electrodes, the resulting electric field in the electrolyte, and the force on the induced charge. (b) A diagram of the resulting bulk flow, with small rolls over the edges of the electrodes and a large roll over the inner edge of the larger electrode that rolls over the others to produce a unidirectional flow.

\*Corresponding author. Email address: ramos@us.es

the electro-osmotic slip velocity, which consists of an oscillatory and a nonzero time-averaged component. For frequencies in the hundreds to kHz range, it is the time-averaged velocity that is observed experimentally and gives rise to the observed fluid flow. The arrangement of coplanar asymmetric electrodes produces a nonsymmetric local flow that eventually generates a global flow in the direction of broken symmetry [9,10].

Figure 1(b) shows a simplified schematic diagram of the fluid flows that occur above the electrodes in the experiments. Rolling motion of the fluid is generated at every electrode edge, the magnitude of the velocity depending on the tangential derivative of the electrical energy stored in the double layer at that location [11,13,14]. The double layer accumulates electrical energy as a capacitor; the normal current to the interface charging the double layer. It is expected that the normal current to the interface and the electrical energy stored in the double layer are more uniform along the small electrode than along the big electrode, since they are distributed over a shorter distance. This results in two rolls over the small electrode, which are of similar size, moving in opposite direction, and, therefore, do not contribute appreciably to the global directional flow. The rolls over the big electrode are more asymmetric, with the higher velocity occurring at the edge closest to the small electrode, where the electric field is stronger. This roll would be limited by the height of the chamber and follow the path shown by the dotted arrow if the chamber were closed at the left and right ends. However, since the chamber is open and the other rolls do not extend upwards to any great height, the fluid instead moves outwards from the inner edge of the large electrode, then up and over the outer edge and the small electrode, and then down towards the next large electrode as shown schematically. This results in a directional flow along the electrode array as seen experimentally [9].

In Ref. [9], it was shown that the fluid flow could be partly accounted for by the analytical theories laid down in Refs. [11,13]. However, the model presented in Ref. [9] was too simple and, if followed strictly, predicted a pumping velocity in the direction opposite to that which is observed experimentally. In this paper, we present a theoretical analysis of the pumping phenomena reported in Ref. [9] in order to predict the direction, and the frequency and voltage dependences of the fluid flow. This is done by using the linear electro-osmotic model presented in Refs. [13,14]. We begin with the presentation of the electrical and mechanical equations, together with the boundary conditions. The electrical equations are then solved numerically using the charge simulation method, taking into account the periodicity of the system in the Green's function. After calculating the electro-osmotic velocity, the stream function of the bulk fluid flow is calculated through an integration of a Green's function for the velocity problem. Finally, the numerical results are presented, paying particular attention to the comparison with the experimental data presented by Brown *et al.*

## II. FORMULATION OF THE PROBLEM

### A. Equations and boundary conditions

The system used to generate the fluid flow is shown by the two-dimensional (2D) geometry depicted in Fig. 2. There

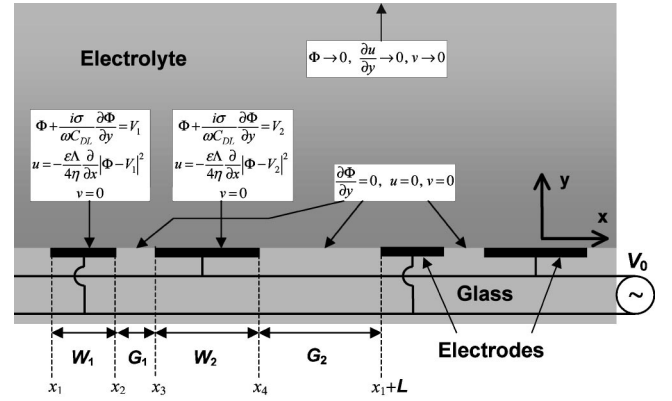


FIG. 2. Cross section of the electrode array showing the asymmetric pairs of electrodes and a summary of the electrical and mechanical boundary conditions.

is an insulating substrate (glass) onto which an infinite periodic array of asymmetric pairs of electrodes is fabricated. The electrodes are considered to be infinitely long and thin, so that any single pair of electrodes can be characterized by widths  $W_1$  and  $W_2$ . The gaps between consecutive electrodes are  $G_1$  and  $G_2$  as shown in the figure. The size of a repeating basic cell is, therefore,  $L = W_1 + G_1 + W_2 + G_2$ . Above the electrode array there is a solution of electrolyte, such as KCl, with conductivity  $\sigma$  and permittivity  $\epsilon$ . At the interfaces between the metal and the electrolyte, and glass and electrolyte, double layers are formed. The characteristic thickness of a double layer is given by the Debye length  $\lambda_D$  [16]. In most cases, this is of the order of 10 nm, and is negligibly small when compared to the other lengths in the system. When an ac voltage is applied to the electrodes, an electrical current is established in the solution. To the first approximation, we assume that the applied voltage is low enough such that electrolysis of the electrolyte does not occur. We also assume that the frequency of the applied signal is low enough, i.e.,  $\omega\epsilon/\sigma \ll 1$ , so that the double layer is in quasiequilibrium [17]. Here,  $\epsilon/\sigma$  is the charge relaxation time of the liquid, and can be viewed as the time an ion takes to travel the Debye length by diffusion:  $\lambda_D^2/D = \epsilon/\sigma$ , where  $D$  is the mean diffusion coefficient of the ions. For periods of the applied signal much greater than the charge relaxation time, the ions can equilibrate locally. Under these conditions, the bulk electrolyte behaves in a resistive manner and the double layer can be considered to behave as an ideal capacitor [17]. Therefore, the electrical potential in the bulk electrolyte satisfies Laplace's equation

$$\nabla^2\Phi = 0. \quad (1)$$

The boundary condition on the electrode surface describes the charging of the double layer due to the current in the bulk,  $\partial q_s/\partial t = -\sigma E_y$ . For sufficiently low voltage, there is a linear relationship between the surface charge and the voltage drop across the double layer. In this case, the surface charge conservation equation can be written using phasors as

$$\sigma \frac{\partial \Phi}{\partial y} = i\omega C_{DL}(\Phi - V_j), \quad (2)$$

where  $C_{DL}$  is the capacitance per unit of area of the total double layer (diffuse plus compact or Stern layers),  $i$  is the imaginary unit,  $\Phi$  is the potential just outside the double layer, and  $V_j$  is the potential applied to electrode  $j$ . At the interface between the electrolyte and the glass, a similar boundary condition holds; however, in this case the boundary condition can be simplified. In the absence of tangential currents, the total normal current (free plus displacement) is continuous,

$$(\sigma + i\varepsilon\omega) \frac{\partial \Phi}{\partial y} = (\sigma_g + i\varepsilon_g\omega) \frac{\partial \Phi_g}{\partial y}, \quad (3)$$

where  $\sigma_g$ ,  $\varepsilon_g$ , and  $\Phi_g$  are, respectively, the electrical conductivity, permittivity, and potential in the glass. Since the conductivity of the glass is negligible, and since the angular frequency  $\omega \ll \sigma/\varepsilon < \sigma/\varepsilon_g$ , the boundary condition on the glass from the liquid side simplifies to

$$\frac{\partial \Phi}{\partial y} = 0. \quad (4)$$

In defining both the boundary conditions, we have implicitly ignored any lateral conduction current along the double layer. The tangential ohmic current flux along the double layer is negligible because it is of the order of  $\lambda_D/l$  times the normal current flux ( $l$  is a typical distance of the system) [13]. Also, any current due to convection in the system has been neglected. This imposes a limit to the validity of the velocity solution. In effect, in order to be consistent the surface charge  $q_s$  that is carried by convection at the double layer should be much smaller than the charge arriving at the electrodes through the normal current,

$$\frac{q_s v}{jl} \sim \frac{q_s v}{\omega q_s l} = \frac{v}{\omega l} \ll 1,$$

where  $v$  is the slip velocity of the fluid. For typical values, the ratio  $v/(\omega l)$  is very small and so the convection current can be neglected safely [13].

The boundary condition at  $y \rightarrow \infty$  is that the potential tends to zero. For a bidimensional problem, this is a correct boundary condition, provided that the total electrical flux at  $x=0$  is zero over a wavelength, i.e.,

$$\int_{-L/2}^{L/2} \frac{\partial \Phi}{\partial y} dx = 0.$$

This ensures that the electrical current cannot extend to infinity.

Owing to electrode polarization [17,18], the electric field in the bulk electrolyte is frequency dependent. When the frequency is low, most of the applied voltage is dropped

across the double layer (across the capacitor). Conversely, when the frequency is high, most of the applied voltage is dropped across the bulk electrolyte. The typical transition frequency can be estimated from simple circuit theory to be  $\omega \sim \sigma/(C_{DL}l)$  [11]. This surface capacitance can be estimated from the Debye-Hückel theory as  $C_{DL} = \varepsilon/\lambda_D$ . The characteristic transition frequency delineating the two extreme conditions is  $\omega \sim (\sigma/\varepsilon)(\lambda_D/l)$ , which is several orders of magnitude smaller than the charge relaxation frequency  $\sigma/\varepsilon$ . Fluid flow due to ac electro-osmosis is observed in the region of this characteristic frequency [9,11,12,14].

Once the electric potential has been solved, the electro-osmotic fluid velocity at the surface of the electrodes can be calculated. For diffuse double layers in quasiequilibrium on perfectly polarizable metal surfaces, the electro-osmotic slip velocity is given by the Helmholtz-Smoluchowski formula [14,19]

$$u = \frac{\varepsilon \Delta \Phi}{\eta} E_x. \quad (5)$$

Here,  $\eta$  is the viscosity of the fluid,  $\Delta \Phi = \Phi - \Phi_0$  is the potential drop across the diffuse double layer ( $\Phi_0$  is the potential at the nonslip plane), and  $E_x$  is the tangential electric field outside the double layer. For our problem, both  $\Delta \Phi$  and  $E_x$  are oscillating functions of time, of frequency  $\omega$ . Therefore, the slip velocity has an oscillating component of frequency  $2\omega$  together with a steady-state component. (There may also be an oscillating component of frequency  $\omega$ , which originates from the product of the intrinsic charge and the applied electric field.) Since the observed fluid flow is driven by the steady-state component [9,12,14], we ignore the others in any further analysis. The time-averaged horizontal fluid velocity at the interface between the double layer and the bulk is [13,14]

$$\langle u \rangle = -\frac{\varepsilon}{4\eta} \Lambda \frac{\partial}{\partial x} [(\Phi - V_j)(\Phi - V_j)^*], \quad (6)$$

where  $*$  indicates the complex conjugate and  $\Lambda$  is the ratio of the diffuse double layer impedance to the total double layer impedance, given by

$$\Lambda = \frac{(i\omega C_d)^{-1}}{(i\omega C_{DL})^{-1}} = \frac{C_d^{-1}}{C_d^{-1} + C_s^{-1}} = \frac{1}{1 + C_d/C_s}, \quad (7)$$

where  $C_d$  and  $C_s$  are the capacitances of the diffuse layer and the Stern or compact layer, respectively. The parameter  $\Lambda$  accounts for the fact that only a fraction of the total voltage present across the double layer is dropped across the diffuse layer. For the glass-electrolyte interface, an estimate of the potential drop across the diffuse double layer shows that this is negligibly small and, from Eq. (5), the electro-osmotic velocity on the glass is negligible [14]. In effect, at the boundary

$$\sigma \frac{\partial \Phi}{\partial y} = i \omega C_{DL} (\Phi - \Phi_g) = i \varepsilon_g \omega \frac{\partial \Phi_g}{\partial y}, \quad (8)$$

taking the second equality, an estimate of the potential drop across the diffuse double layer on the glass is

$$\Phi - \Phi_g = \frac{\varepsilon_g}{C_{DL}} \frac{\partial \Phi_g}{\partial y} \sim \frac{\varepsilon_g \lambda_D}{\varepsilon l} \Phi_g, \quad (9)$$

which is of the order of  $\lambda_D$  divided by the typical distance of the system,  $l$ .

To obtain the velocity in the bulk, the Navier-Stokes equations must be solved. For microsystems, the Reynolds number is usually very small, so that the inertial terms in the Navier-Stokes equations can be neglected. In the steady state, and in the absence of externally applied body forces, the equations reduce to

$$\eta \nabla^2 \mathbf{u} - \nabla p = 0, \quad \nabla \cdot \mathbf{u} = 0, \quad (10)$$

where  $p$  is the pressure and  $\mathbf{u}$  the velocity,  $\mathbf{u} = u \mathbf{e}_x + v \mathbf{e}_y$ . The boundary conditions for these equations at  $y=0$  are (a) the tangential velocity is equal to the slip velocity on the electrodes, given by Eq. (6); (b) the tangential velocity is zero at the glass; and (c) the normal velocity is zero for any  $x$  at  $y=0$  (electrodes and glass). Far from the electrodes in the normal direction, the fluid can be considered to be free of stress, where  $\partial u / \partial y = 0$  and  $v = 0$ . Given the periodicity of the electrode array, we look for periodic solutions in the  $x$  direction. A summary of the electrical and mechanical boundary conditions is shown in Fig. 2.

If a net fluid flow occurs, the velocity tends to  $\mathbf{u} = U \mathbf{e}_x$  for  $y \rightarrow \infty$ , where  $U$  is a constant. This boundary condition presumes that the upper boundary of any actual device is very much higher than the wavelength of the problem. To obtain the velocity profile of the outer region, Eq. (10) has to be solved with  $\mathbf{u} = U \mathbf{e}_x$  as the boundary condition for the lower boundary.

Net flow in a periodic array of microelectrodes will occur if the average value of the slip velocity over a wavelength is nonzero, i.e.,

$$U = \frac{1}{L} \int_{-L/2}^{L/2} u \, dx \neq 0. \quad (11)$$

This equality can be proved by solving Eq. (10) in the  $x$  direction using Fourier analysis. The Fourier component of the velocity that produces net flow in the longitudinal direction is the component with zero wave number, the constant component. The theoretical model presented in Ref. [9] does not take this into account, and in fact, the model predicts a velocity in a direction opposite to that which is observed in practice; from left to right in Fig. 2. Here, we show that by solving the equations presented in this paper, the predicted direction of the fluid flow coincides with experimental observations.

## B. General analysis of the solution

The pumping velocity  $U$  for an array of pairs of asymmetric electrodes as shown in Fig. 2 is

$$\begin{aligned} U &= \frac{1}{L} \left( \int_{x_1}^{x_2} u \, dx + \int_{x_3}^{x_4} u \, dx \right) \\ &= -\frac{\varepsilon \Lambda}{4 \eta L} \left( \int_{x_1}^{x_2} \frac{\partial}{\partial x} |\Phi - V_1|^2 dx + \int_{x_3}^{x_4} \frac{\partial}{\partial x} |\Phi - V_2|^2 dx \right) \\ &= -\frac{\varepsilon \Lambda}{4 \eta L} (|\Phi - V_1|_{x_2}^2 - |\Phi - V_1|_{x_1}^2 + |\Phi - V_2|_{x_4}^2 \\ &\quad - |\Phi - V_2|_{x_3}^2), \end{aligned} \quad (12)$$

where  $x_1$  and  $x_2$  are the positions of the edges of electrode 1, and  $x_3$  and  $x_4$  the positions of the edges of electrode 2, therefore,  $x_2 - x_1 = W_1$ ,  $x_3 - x_2 = G_1$ ,  $x_4 - x_3 = W_2$ , and  $x_1 + L - x_4 = G_2$ .

According to Eq. (12), the pumping velocity depends on the values of  $|\Phi - V_j|^2$  at the electrode edges. Without loss of generality, we can choose  $x_1 = 0$ , so that  $x_2 = W_1$ ,  $x_3 = W_1 + G_1$ , and  $x_4 = W_1 + G_1 + W_2$ . It is convenient to scale lengths with  $W_2$ , and potentials with the applied potential difference  $V_0 = V_2 - V_1$ . The electrical problem depends only on four independent nondimensional parameters:  $\tilde{W}_1 = W_1 / W_2$ ,  $\tilde{G}_1 = G_1 / W_2$ ,  $\tilde{G}_2 = G_2 / W_2$ , and  $\Omega = C_{DL} \omega W_2 / \sigma$ . The parameter  $\Omega$  comes from the boundary condition given by Eq. (2). The pumping velocity is therefore

$$\begin{aligned} U &= -\frac{\varepsilon V_0^2}{4 \eta L} \Lambda (|\tilde{\Phi} - \tilde{V}_1|_{x_2}^2 - |\tilde{\Phi} - \tilde{V}_1|_0^2 + |\tilde{\Phi} - \tilde{V}_2|_{x_4}^2 \\ &\quad - |\tilde{\Phi} - \tilde{V}_2|_{x_3}^2), \end{aligned} \quad (13)$$

where variables with tilde are reduced or nondimensional quantities. This equation shows us that the product  $(\eta L U) / (\varepsilon V_0^2 \Lambda)$  depends only on  $\tilde{W}_1$ ,  $\tilde{G}_1$ ,  $\tilde{G}_2$ , and  $\Omega$ . For a given value of the applied voltage, the maximum value of the product  $UL$  as a function of frequency depends on  $\tilde{W}_1$ ,  $\tilde{G}_1$ , and  $\tilde{G}_2$ . Therefore, the same value for the maximum  $UL$  is obtained for  $(W_1, W_2, G_1, G_2)$  and for  $(\alpha W_1, \alpha W_2, \alpha G_1, \alpha G_2)$ . Since  $UL$  is constant in this transformation, the pumping velocity increases as the wavelength decreases. Greater velocities are obtained if the unit cell size is reduced or, equivalently, if the number of cells per array length is increased. In principle, the validity of this result is restricted to the validity of the approximations made in the derivation, i.e.,  $\lambda_D / l \ll 1$ ,  $\omega \varepsilon / \sigma \ll 1$ , and  $u / (\omega l) \ll 1$ .

## C. Electrical problem

The electrical potential can be numerically solved for the periodic array using the surface charge simulation method [20,21]. The method seeks to find charges distributed over the boundaries that generate the potential solution in the domain of interest. The periodicity of the system can be taken

into account by considering the potential generated by an infinite array of parallel source lines. According to Ref. [22], the potential due to a uniform grid of source lines of unit value, with spacing  $L$  along the  $x$  axis at positions  $x=0, \pm L, \pm 2L, \pm 3L, \dots$ , is

$$\phi(x,y) = -\frac{1}{4\pi\epsilon} \ln[\sinh^2(ky/2) + \sin^2(kx/2)], \quad (14)$$

where  $k=2\pi/L$ . The potential created by a periodic surface charge distribution of period  $L$  placed at  $y=0$  is, therefore,

$$\Phi(x,y) = \int_{-L/2}^{L/2} dx' q_s(x') \phi(x-x',y). \quad (15)$$

Since the surface charge is related to the normal derivative of the potential at  $y=0^+$  through  $q_s/(2\epsilon) = -\partial\Phi/\partial y$ , we can write for  $y>0$ ,

$$\begin{aligned} \Phi(x,y) = & \frac{1}{2\pi} \int_{-L/2}^{L/2} dx' \Phi_y(x',0) \ln\{\sinh^2(ky/2) \\ & + \sin^2[k(x-x')/2]\}, \end{aligned} \quad (16)$$

where  $\Phi_y(x',0) = \partial\Phi/\partial y$  at  $y=0^+$ . The function

$$G(x-x',y) = \frac{1}{2\pi} \ln\{\sinh^2(ky/2) + \sin^2[k(x-x')/2]\} \quad (17)$$

is the Green's function that satisfies  $\nabla^2 G=0$  for  $y>0$  subjected to the condition  $\partial G/\partial y = \sum_{n=-\infty}^{\infty} \delta(x-x'-nL)$  at  $y=0^+$ .

Putting  $y=0$  in Eq. (16), we arrive at the first equation required for the numerical solution,

$$\Phi(x,0) = \frac{1}{2\pi} \int_{-L/2}^{L/2} dx' \Phi_y(x',0) \ln\{\sin^2[k(x-x')/2]\}. \quad (18)$$

This equation relates the potential at  $y=0$  to the normal derivative at  $y=0$ , and together with the boundary condition, is the governing equation for  $\Phi_y$  that has to be solved numerically.

If, instead of a periodic array, a finite number of electrodes is considered, the equation equivalent to Eq. (16) is

$$\Phi(x,y) = \frac{1}{2\pi} \int_{-\infty}^{\infty} dx' \Phi_y(x') \ln[(x-x')^2 + y^2], \quad (19)$$

where the potential solution for a charge line placed at  $x=x', y=0$  has been used [20,21].

#### D. Velocity problem

The Fourier components of the time-averaged velocity and pressure are

$$u = \sum_{n=-\infty}^{\infty} u_n(y) e^{ik_n x}, \quad v = \sum_{n=-\infty}^{\infty} v_n(y) e^{ik_n x},$$

$$p = \sum_{n=-\infty}^{\infty} p_n(y) e^{ik_n x}, \quad (20)$$

where  $k_n = nk = 2n\pi/L$  and  $n$  is an integer. The Stokes equations [Eq. (10)] require that

$$ik_n u_n + \frac{\partial v_n}{\partial y} = 0, \quad (21)$$

$$\eta \left( -k_n^2 u_n + \frac{\partial^2 u_n}{\partial y^2} \right) - ik_n p_n = 0, \quad (22)$$

$$\eta \left( -k_n^2 v_n + \frac{\partial^2 v_n}{\partial y^2} \right) - \frac{\partial p_n}{\partial y} = 0, \quad (23)$$

and the boundary conditions at  $y=0$  and  $y \rightarrow \infty$  require that

$$u_n(0) = \frac{1}{L} \int_{-L/2}^{L/2} u(x,0) e^{-ik_n x} dx, \quad (24)$$

$$v_n(0) = 0, \quad (25)$$

$$\lim_{y \rightarrow \infty} \frac{\partial u_n}{\partial y} = 0, \quad (26)$$

$$\lim_{y \rightarrow \infty} v_n(y) = 0, \quad (27)$$

where  $u(x,0)$  is either the slip velocity at the electrodes [Eq. (6)] or zero at the glass. Combining the Stokes equations for the Fourier components, it can be shown that

$$\left( \frac{\partial^2}{\partial y^2} - k_n^2 \right)^2 u_n(y) = 0, \quad (28)$$

$$\left( \frac{\partial^2}{\partial y^2} - k_n^2 \right)^2 v_n(y) = 0, \quad (29)$$

$$\left( \frac{\partial^2}{\partial y^2} - k_n^2 \right) p_n(y) = 0. \quad (30)$$

The solution of these equations that satisfy the boundary conditions is

$$u = \sum_{n=-\infty}^{\infty} u_n(0) (1 - |k_n|y) e^{-|k_n|y + ik_n x}, \quad (31)$$

$$v = -i \sum_{n=-\infty}^{\infty} u_n(0) k_n y e^{-|k_n|y + ik_n x}, \quad (32)$$

$$p = -i2\eta \sum_{n=-\infty}^{\infty} u_n(0)k_n e^{-|k_n|y + ik_n x}. \quad (33)$$

The only Fourier component of the velocity that creates a nonzero net flow [ $\int_0^\infty u_n(y)dy \neq 0$ ] is  $u_0(0) \equiv U$  [23]. Therefore, the first objective is to find  $U$  for a given electrode array.

Defining the stream function  $\Psi$  by the pair of derivatives  $\partial\Psi/\partial y = u$  and  $\partial\Psi/\partial x = -v$ , we have

$$\Psi = \sum_{n=-\infty}^{\infty} u_n(0)y e^{ik_n x - |k_n|y}. \quad (34)$$

The stream function can be elaborated further by inserting the definition of  $u_n(0)$ ,

$$\Psi = \frac{1}{L} \int_{-L/2}^{L/2} dx' u(x', 0) y \sum_{n=-\infty}^{\infty} e^{ik_n(x-x') - |k_n|y}. \quad (35)$$

The series can be summed by considering that  $\sum_{n=1}^{\infty} r^n = r/(1-r)$  for  $|r| < 1$ , and  $r_{\pm} = \exp[k(\pm i(x-x') - y)]$ . The result is

$$\Psi = \frac{1}{L} \int_{-L/2}^{L/2} dx' u(x', 0) \frac{y \sinh(ky)}{\cosh(ky) - \cos[k(x-x')]}. \quad (36)$$

Following some manipulation

$$\Psi = \int_{-L/2}^{L/2} dx' u(x', 0) y \frac{\partial G(x-x', y)}{\partial y}, \quad (37)$$

where the function  $G$  was defined in Eq. (17). Therefore, we can obtain the stream function for the velocity in the bulk through an integral of the slip velocity previously calculated multiplied by  $H(x-x', y) = y \partial G / \partial y$ . Thus,  $H$  is the Green's function for the stream function in our problem. A physical interpretation of  $H$  is that it represents the stream function of an array of velocity source lines with spacing  $L$  along the  $x$  axis at positions  $x = x' + nL$ . At  $y=0$ , these velocity sources satisfy

$$v(x) = 0, \quad (38)$$

$$u(x) = \sum_{n=-\infty}^{\infty} \delta(x-x'-nL).$$

Figure 3 shows a plot of the stream function  $H$  for the case  $x'=0$ , and  $L=1$ . For  $ky \gg 1$ ,  $H$  tends to  $y/L$  i.e., the streamlines are parallel to the  $x$  axis. In the neighborhood of  $x=x'$ ,  $y=0$ , the stream function  $H$  takes the form

$$H = \frac{1}{\pi} \frac{y^2}{y^2 + (x-x')^2} = \frac{\sin^2 \alpha}{\pi}, \quad (39)$$

where  $\alpha$  is the angle in polar coordinates with the origin at  $x=x'$ ,  $y=0$ . The streamlines are radial lines in this neighborhood and the flow is inwards for  $0 < \alpha < \pi/2$  and out-

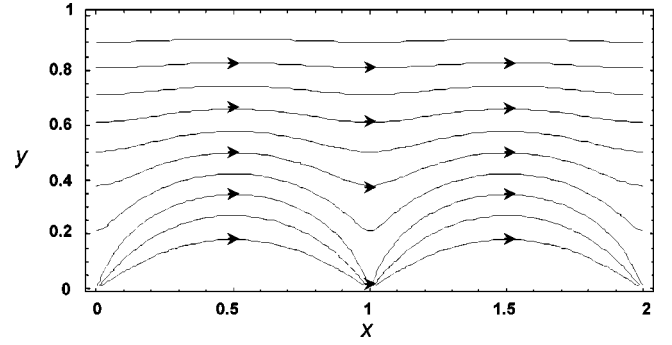


FIG. 3. Streamlines for an array of velocity source lines.

wards for  $\pi/2 < \alpha < \pi$ . Experimentally,  $H$  represents the limiting case for the stream function generated by an array of electrodes where the electro-osmotic slip velocity is only nonzero in a small region of each pair of electrodes.

### III. NUMERICAL ANALYSIS

The starting point is Eq. (18), which defines the potential at  $y=0$ ,  $\Phi(x,0)$ , as an integral of the normal derivative of the potential at  $y=0$  multiplied by the Green's function. This equality can be viewed as the potential created by a periodic surface charge distribution placed at  $y=0$ . In our problem, both the real and the imaginary parts of the potential satisfy Eq. (18).

We now apply the boundary conditions given by Eqs. (2) and (4) to Eq. (18) to give

$$V_1 + \frac{1}{i\Omega} \Phi_y(x) = \int_{x_1}^{x_2} g(x-x') \Phi_y(x') dx' + \int_{x_3}^{x_4} g(x-x') \times \Phi_y(x') dx' \quad \text{for } x \in (x_1, x_2) \quad (40)$$

and

$$V_2 + \frac{1}{i\Omega} \Phi_y(x) = \int_{x_1}^{x_2} g(x-x') \Phi_y(x') dx' + \int_{x_3}^{x_4} g(x-x') \times \Phi_y(x') dx' \quad \text{for } x \in (x_3, x_4), \quad (41)$$

where

$$g(x-x') = G(x-x', 0) = \frac{1}{2\pi} \ln \left[ \sin^2 \left( \frac{\pi(x-x')}{L} \right) \right]. \quad (42)$$

The unknown parameter is the function  $\Phi_y(x)$  over each electrode.  $V_1$  and  $V_2$  are not given individually, only the difference  $V_0$  is fixed. One additional condition is needed to complete the problem, and this is that the current flows from one electrode to the other, i.e., the total flux of current through the plane  $y=0$  is zero. These two conditions are expressed through the relations

$$V_2 - V_1 = V_0, \quad (43)$$

$$\int_{x_1}^{x_2} \Phi_y(x') dx' + \int_{x_3}^{x_4} \Phi_y(x') dx' = 0. \quad (44)$$

The set of equations (40), (41), (43), and (44) was solved numerically using the Galerkin method. In order to represent the function  $\Phi_y(x)$  on each electrode, two types of basic functions were used: the Legendre polynomials and the piecewise constant functions. Both techniques gave very similar results.

Let us define  $f_1(x)$  as the Galerkin approximation to the normal derivative of the potential for points on electrode 1,  $x \in (x_1, x_2)$ , and  $f_2(x)$  as the approximation to this normal derivative at electrode 2,  $x \in (x_3, x_4)$ . The functions  $f_1$  and  $f_2$  are written as

$$f_1(x) = \sum_{j=1}^{N_1} C_{1j} w_{1j}(x),$$

$$f_2(x) = \sum_{j=1}^{N_2} C_{2j} w_{2j}(x), \quad (45)$$

where  $w_{1j}$  and  $w_{2j}$  are the basic functions.

The equations for the Galerkin approximation are

$$0 = - \int_{x_1}^{x_2} dx \left( V_1 + \frac{1}{i\Omega} f_1(x) \right) w_{1j}(x)$$

$$+ \int_{x_1}^{x_2} dx \int_{x_1}^{x_2} dx' g(x-x') f_1(x') w_{1j}(x)$$

$$+ \int_{x_1}^{x_2} dx \int_{x_3}^{x_4} dx' g(x-x') f_2(x') w_{1j}(x),$$

$$j = 1, \dots, N_1, \quad (46)$$

$$0 = - \int_{x_3}^{x_4} dx \left( V_2 + \frac{1}{i\Omega} f_2(x) \right) w_{2j}(x)$$

$$+ \int_{x_3}^{x_4} dx \int_{x_1}^{x_2} dx' g(x-x') f_1(x') w_{2j}(x)$$

$$+ \int_{x_3}^{x_4} dx \int_{x_3}^{x_4} dx' g(x-x') f_2(x') w_{2j}(x),$$

$$j = 1, \dots, N_2. \quad (47)$$

This discrete set of equations, together with Eqs. (43) and (44) represent the complete set of equations required to define the unknowns  $C_{1j}$ ,  $C_{2j}$ ,  $V_1$ , and  $V_2$ . In the Appendix, the technique used to perform the Galerkin integrations is described.

In order to test the numerical solutions and estimate the error of the present numerical results, we compared the results with some representative finite-element solutions. In Ref. [24], the electrical potential generated by an interdigitated electrode array was numerically calculated using the finite-element method. In these computations, the electrodes had a fixed value of the potential. In our problem, the bound-

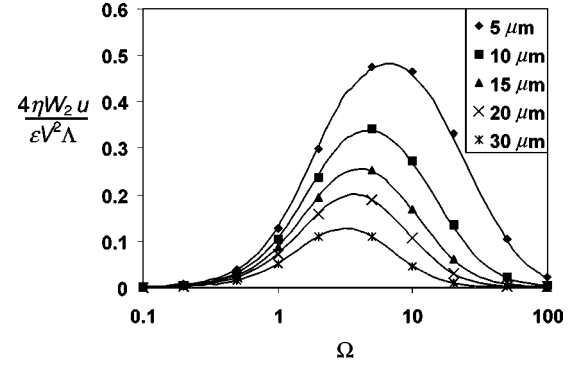


FIG. 4. Reduced slip velocity  $4\eta W_2 u / \varepsilon V_0^2 \Lambda$  versus nondimensional frequency  $\Omega$  at several positions on the electrode for  $W_2 = W_1 = 100 \mu\text{m}$ ,  $G_1 = 25 \mu\text{m}$ ,  $G_2 = 10^3 W_1$ . Points give numerical results from Ref. [14]; solid lines give results from this work.

ary condition given by Eq. (2) reduces to this when  $\Omega$  goes to infinity. The electrical potential for  $y \rightarrow \infty$  is of the form  $A e^{-ky}$ . A comparison of the values of the constant  $A$  obtained in the present work with those from the finite-element method shows a discrepancy smaller than 0.15%. These results were obtained for a high value of  $\Omega$  using  $n = 18$  Legendre polynomials. Therefore, we believe that the results presented in this paper are correct with an estimated error smaller than 0.2%.

The numerically calculated values for the velocity were also compared with numerical results published previously. In Ref. [14], the slip velocity produced by a pair of symmetric electrodes was calculated using the finite-element method. Figure 4 shows the reduced velocity  $4\eta W_2 u / \varepsilon V_0^2 \Lambda$  versus the nondimensional frequency  $\Omega$  for different positions on the electrodes, measured from the edge close to the gap. The electrode widths are  $W_1 = W_2 = 100 \mu\text{m}$ , and the gap between them is  $G_1 = 25 \mu\text{m}$ . For the sake of comparison, the other gap  $G_2$  was chosen to be very large,  $G_2 = 10^3 W_1$ , for these calculations. The figure shows that the different methods for calculating the flow velocity agree perfectly.

#### IV. RESULTS AND DISCUSSION

In the following section, for the sake of simplicity, reduced quantities will be used, except where otherwise stated. Lengths are scaled with  $W_2$ , voltages are scaled with  $V_0$ , and velocities are measured in units of  $(\varepsilon V_0^2 \Lambda) / (4\eta W_2)$ .

Unidirectional fluid flow only occurs if the electrode pair in the array is asymmetric, and again the flow velocity is a function of frequency. The derivative of  $|\Phi - V|^2$  with respect to  $x$  gives the slip velocity on each electrode. Figure 5 shows the function  $|\Phi - V|^2$  for each electrode of a unit cell, where  $V_0 = 1$ ,  $W_1 = G_1 = 0.3$ ,  $W_2 = G_2 = 1$ , and  $\Omega = 4.12$ . This is the frequency of maximum velocity for this particular electrode array. The function  $|\Phi - V|^2$  is plotted against  $x/W_i$ , the position on the electrode scaled with the electrode width, so that  $x/W_i = 0$  is the left edge and  $x/W_i = 1$  is the right edge. Although  $|\Phi - V|^2$  is much greater at the narrow electrode than at the wide electrode, its derivative is not.

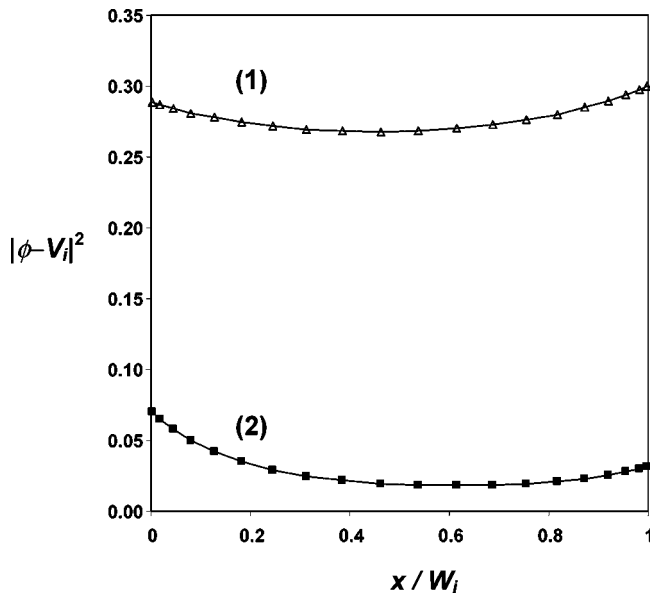


FIG. 5. The function  $|\Phi - V|^2$  on top of the electrodes for the case  $W_1 = G_1 = 0.3$ ,  $W_2 = G_2 = 1$ ,  $V_0 = 1$ ,  $\Omega = 4.12$ . Curve 1, narrow electrode; curve 2, wide electrode.

According to Eq. (13), the difference in the values of  $|\Phi - V|^2$  at the edges gives the pumping velocity. The net flow over the narrow electrode is to the left, while the flow over the wide electrode is to the right. Figure 6 shows the slip velocity  $u(x)$  on each electrode of the cell. The slip velocity is more symmetrical over the narrow electrode, resulting in a smaller pumping effect than for the wide electrode, i.e.,  $|\int_{x_1}^{x_2} u dx| < |\int_{x_3}^{x_4} u dx|$ . Net fluid flow occurs in the direction from the narrow electrode to the nearest wide one, i.e., to the right in Fig. 2. This is the direction observed in experiments [9]. Here, we note that the potential difference  $|\Phi - V|$  is more evenly distributed in the narrow electrode, which reduces the pumping effect of that electrode. The cur-

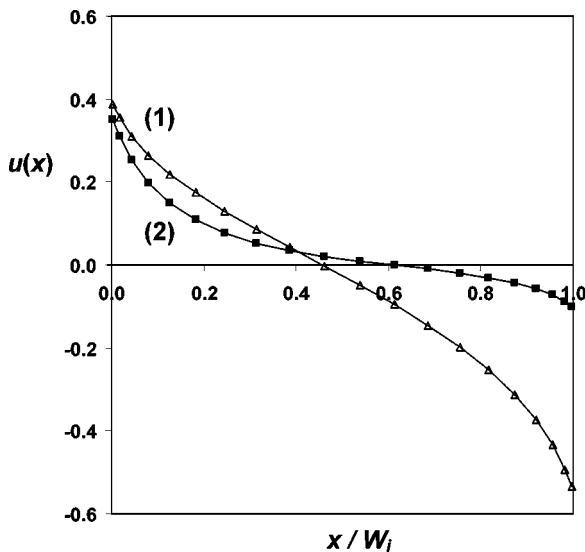


FIG. 6. The slip-velocity function  $u(x)$  on top of the electrodes for the case  $W_1 = G_1 = 0.3$ ,  $W_2 = G_2 = 1$ ,  $V_0 = 1$ ,  $\Omega = 4.12$ . Curve 1, narrow electrode; curve 2, wide electrode.

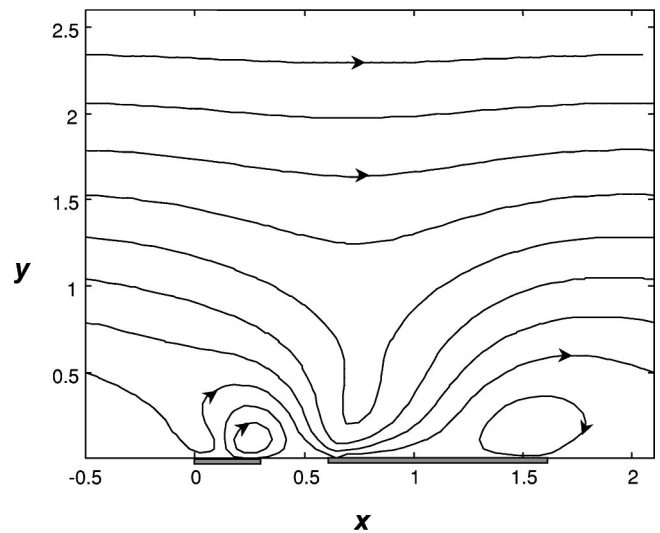


FIG. 7. Streamlines of the fluid velocity field for the case  $W_1 = G_1 = 0.3$ ,  $W_2 = G_2 = 1$ ,  $V_0 = 1$ ,  $\Omega = 4.12$ .

rent that arrives at a narrow electrode should be more evenly distributed than for a wide electrode because this is a way of reducing the electrical resistance. Since  $\Phi - V$  is proportional to  $\sigma\Phi_y$ , it follows that at the narrow electrode the pumping effect is smaller than at the wide electrode. The model presented by Brown *et al.* predicts a greater pumping effect on the narrow electrode than on the wide one because the current distribution between electrodes was assumed rather than solved. This gave a current on the narrow electrode that was not as evenly distributed as in reality. Figure 7 shows the streamlines produced by these slip velocity functions over the electrodes. The arrows indicate the direction of the fluid flow. It shows that at sufficient height, the fluid velocity is constant and the streamlines are parallel to the  $x$  axis. For the sake of comparison, Fig. 8 shows the streamlines for a symmetrical electrode array. It shows that there is no net flow because the array is symmetric. At the level of the electrodes, the flow direction is from the edges to the center of each electrode as observed experimentally [12,14].

Figure 9 shows the pumping velocity  $U$  as a function of frequency  $\Omega$  for the asymmetric array with  $W_1 = G_1 = 0.3$ ,  $W_2 = G_2 = 1$ , and  $V_0 = 1$ . The velocity-frequency curve has a bell shape. The maximum occurs at  $\Omega = 4.12$  and has a value

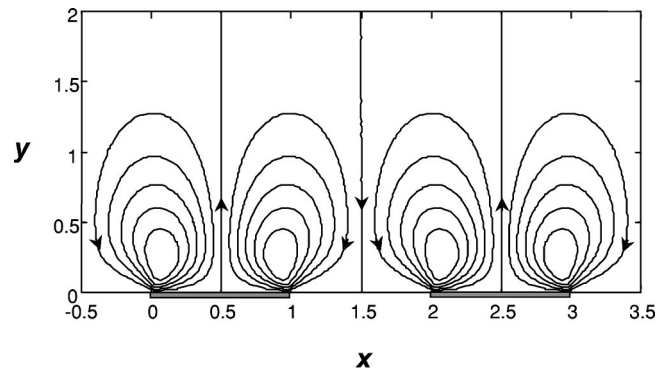


FIG. 8. Streamlines of the fluid velocity field for the case  $W_1 = W_2 = G_1 = G_2 = 1$ ,  $V_0 = 1$ ,  $\Omega = 10$ .



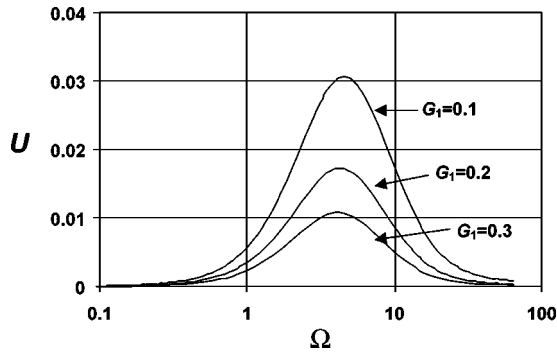


FIG. 9. Pumping velocity  $U$  versus nondimensional frequency  $\Omega$  for  $W_1=0.3$ ,  $W_2=G_2=1$ ,  $V_0=1$ , and different values of  $G_1$ .

of  $U=0.0108$ . Figure 9 also shows the same function  $U = U(\Omega)$ , but with different values of gap  $G_1$  between electrodes. As  $G_1$  decreases, the maximum velocity increases for fixed values of  $W_1$ ,  $W_2$ ,  $G_2$ , and  $V_0$ .

Figure 10(a) shows  $U$  multiplied by  $L$  as a function of gap  $G_2$  for  $G_1=W_1=0.3$ ,  $W_2=1$ , and  $\Omega=5$ .  $G_2$  is the separation between a pair of electrodes. This figure shows that  $UL$  has a maximum value for infinite separation  $G_2$ . When  $G_2 = G_1=0.3$ , the velocity is zero; in this case there is a left-right symmetry and no preferential direction of flow. If  $G_2 < G_1$ , the velocity changes sign. This should be obvious since, in this case, the smallest gap is now  $G_2$  and is between a wide electrode on the left and a narrow electrode on the right. In Fig. 10(b), the velocity  $U$  is plotted as a function of the separation  $G_2$ , with other parameters as for Fig. 10(a). A maximum in velocity now occurs for  $G_2 \approx 1$ .

Brown *et al.* [9] presented experimental results showing how the pumping velocity varied as a function of frequency and voltage. Their experimental array of interdigitated electrodes had the following dimensions: electrode widths of  $W_1=4.2 \mu\text{m}$  and  $W_2=25.7 \mu\text{m}$ , and gaps of  $G_1=4.5 \mu\text{m}$  and  $G_2=15.6 \mu\text{m}$ . The electrolyte had a conductivity of  $\sigma = 1.23 \times 10^{-3} \text{ S m}^{-1}$ , giving a Debye length of 30 nm. Using

nondimensional variables, these parameters can be rewritten as  $W_1=0.1634$ ,  $W_2=1$ ,  $G_1=0.1751$ ,  $G_2=0.6070$ , and  $V_0=1$ . The numerically calculated maximum velocity is then  $U_{max}=0.01888$ , and this occurs at a frequency of  $\Omega = 6.3973$ . For  $\Lambda=1$  (no compact layer), the corresponding dimensional velocity is  $U_{max}=257.6 V_{rms}^2 \mu\text{m/s}$ , where  $V_{rms}$  is the rms applied voltage. The experimental value given by Brown *et al.* was around 2.7 times smaller,  $U_{max} = 95 V_{rms}^2 \mu\text{m/s}$ . An estimation of the surface capacitance can be made from  $C_{DL} = \epsilon/\lambda_D$ , and this gives a frequency of maximum velocity of  $f = (1/2\pi)(\sigma/\epsilon)(\lambda_D/W_2)\Omega = 2.08 \text{ kHz}$ , compared to a measured value of 2.9 kHz at low voltages. The existence of a compact layer at the electrode surface would reduce the predicted velocity and increase the predicted frequency. The experimental values are obtained if the capacitances of the diffuse layer,  $C_d$ , and the compact layer,  $C_s$ , are set equal to  $C_d = 1.9\epsilon/\lambda_D$  and  $C_s = 0.9\epsilon/\lambda_D$ . The calculated streamlines for the electrode array used by Brown *et al.* are very similar to those of Fig. 7. The rolls that form on top of the electrodes resemble the sketch of flow profile given in Ref. [9].

The numerical solution can be used to determine the optimum values of gap and width for the electrodes used by Brown *et al.* As discussed previously, reducing  $G_1$  causes the velocity to increase, therefore we have calculated the pumping velocity for fixed  $G_1=0.1751$  and  $W_2=1$ . Setting  $W_1$  to 0.1634, an optimum value for  $G_2$  is found, which is shown in Fig. 11(a). Each point of this figure gives the maximum velocity as a function of frequency for a given  $G_2$ . The figure shows that the optimum value of  $G_2$  is around 0.7. However, the maximum is not very pronounced, and between  $G_2=0.5$  and  $G_2=1.2$  the difference is  $\approx 5\%$  or less. An alternative approach is to set  $G_2$  to 0.607, so that an optimum value of  $W_1$  can be found. In Fig. 11(b), the maximum velocity  $U_{max}$ , calculated as a function of frequency for each value of  $W_1$  is plotted against  $W_1$ . The optimum value of  $W_1$  is found to be between  $W_1=0.2$  and 0.25. The

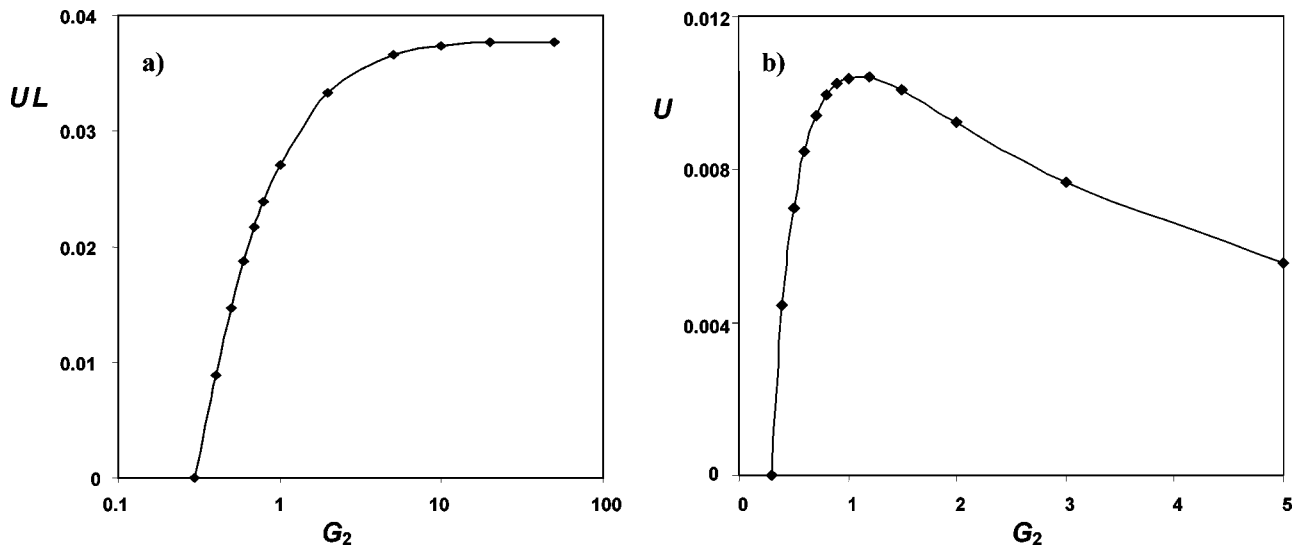


FIG. 10. (a) Pumping velocity  $U$  multiplied by wavelength  $L$  versus  $G_2$  and (b) pumping velocity  $U$  versus  $G_2$ . Case:  $W_1=G_1=0.3$ ,  $W_2=1$ ,  $\Omega=5$ .

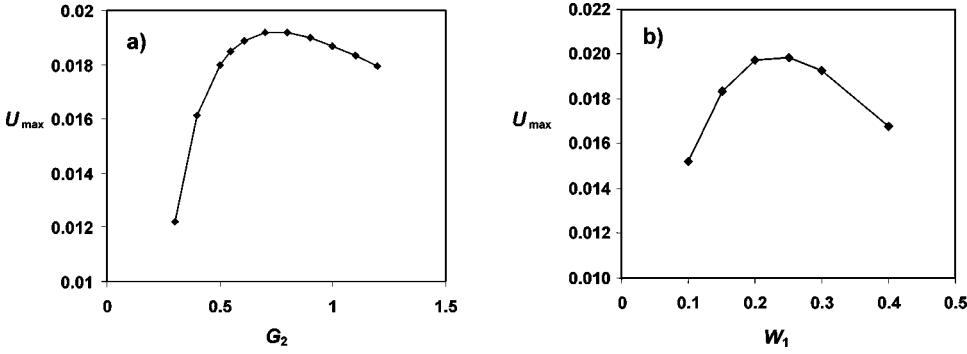


FIG. 11. (a) Maximum pumping velocity  $U_{max}$  as a function of  $G_2$  for  $W_1=0.1634$ ,  $G_1=0.1751$ ,  $W_2=1$ . (b) Maximum pumping velocity  $U_{max}$  as a function of  $W_1$  for  $G_1=0.1751$ ,  $W_2=1$ ,  $G_2=0.6070$ .

difference with respect to the peak velocity is less than 8% for values of  $W_1$  between 0.15 and 0.35. The value of  $U_{max}=0.01888$  obtained using the experimental sizes is around 8% from a maximum value  $U_{max}=0.0204$  obtained with  $W_1=0.24$  and  $G_2=0.8$ .

## V. CONCLUSIONS

A theoretical analysis of the electro-osmotic pumping generated by an ac electric potential applied to an array of asymmetric pairs of microelectrodes has been presented. The interaction between the oscillating electric field and the oscillating induced charge at the diffuse double layer on the electrodes results in a steady electro-osmotic velocity distribution on top of the electrodes. The broken left-right symmetry of the system produces a nonsymmetric slip velocity distribution that drives a net fluid flow.

The electrical equations have been solved numerically using the charge simulation method. The periodic nature of the system has been taken into account in the Green's function, so that only the unit cell of length  $L$  has to be considered. The stream function of the bulk flow generated by the electro-osmotic slip velocity has been calculated.

The fluid flow dependence on voltage and frequency have been described. Optimum values for the nondimensional parameters  $G_2$ ,  $W_1$  have been calculated in order to obtain greater pumping velocities. A comparison with the experiments reported by Brown *et al.* has been made and a good agreement has been found.

## ACKNOWLEDGMENTS

The authors would like to thank the Spanish government agency Dirección General de Ciencia y Tecnología under Contract No. BFM2000-1056, the Royal Academy of Engineering UK, and the Royal Society for funding.

## APPENDIX

The integrations that appear in the method of Galerkin using the Legendre polynomials are of the form

$$\begin{aligned} & \int_{x_1}^{x_2} dx \int_{x_1}^{x_2} dx' g(x-x') P_m(x) P_n(x') \\ &= \left( \frac{x_2-x_1}{2} \right)^2 \int_{-1}^1 ds \int_{-1}^1 ds' g(x-x') P_m(s) P_n(s'), \end{aligned}$$

where  $x = \frac{1}{2}(x_2-x_1)s + \frac{1}{2}(x_2+x_1)$ ,  $x' = \frac{1}{2}(x_2-x_1)s' + \frac{1}{2}(x_2+x_1)$ ;

$$\begin{aligned} & \int_{x_1}^{x_2} dx \int_{x_3}^{x_4} dx' g(x-x') P_m(x) P_n(x') \\ &= \frac{(x_2-x_1)(x_4-x_3)}{4} \int_{-1}^1 ds \int_{-1}^1 ds' g(x-x') \\ & \quad \times P_m(s) P_n(s'), \end{aligned}$$

where  $x = \frac{1}{2}(x_2-x_1)s + \frac{1}{2}(x_2+x_1)$ ,  $x' = \frac{1}{2}(x_4-x_3)s' + \frac{1}{2}(x_4+x_3)$ .

In the first case, the singularity that occurs when  $s=s'$  should be taken into account. In the second case, it is always  $x(s) \neq x'(s')$  and the integration can be done numerically without much problem. The singularity at  $s=s'$  is of the form  $\ln(s-s')^2$ . We can write

$$\begin{aligned} & \int_{-1}^1 \int_{-1}^1 ds ds' g(x-x') P_m(s) P_n(s') \\ &= \int_{-1}^1 \int_{-1}^1 ds ds' \ln \left( \frac{\sin^2[k(x-x')/2]}{(s-s')^2} \right) P_m(s) P_n(s') \\ & \quad + \int_{-1}^1 \int_{-1}^1 ds ds' \ln[(s-s')^2] P_m(s) P_n(s'). \quad (\text{A1}) \end{aligned}$$

The first integral on the right-hand side is done numerically since the integrand is not singular. The integral with the singularity is done analytically. A repeated use of the formula

$$\begin{aligned} & \int_{-1}^1 dt t^n \ln|x-t| = \frac{1-x^{n+1}}{n+1} \ln|1-x| - \frac{(-1)^{n+1}-x^{n+1}}{n+1} \\ & \quad \times \ln|1+x| - \sum_{k=0}^n \frac{1-(-1)^{n+1}}{(n+1)(k+1)} x^{n-k} \quad (\text{A2}) \end{aligned}$$

is employed to obtain the value of the integral  $\int_{-1}^1 \int_{-1}^1 ds ds' s^m (s')^n \ln[(s-s')^2]$ . This together with the coefficients of the Legendre polynomials allow us to compute the required integral  $\int_{-1}^1 \int_{-1}^1 ds ds' \ln[(s-s')^2] P_m(s) P_n(s')$ .

- [1] *Micro Total Analysis Systems 2001*, edited by J.M. Ramsey and A. van den Berg (Kluwer Academic, Dordrecht, 2001).
- [2] C.M. Ho, and Y.C. Tai, *Annu. Rev. Fluid Mech.* **30**, 579 (1998).
- [3] G.M. Whitesides and A. Stroock, *Phys. Today* **54**, 42 (2001).
- [4] H.T.G. van Lintel, *Sens. Actuators* **15**, 153 (1988).
- [5] A. Manz, C.S. Effenhauser, N. Burggraf, D.J. Harrison, K. Seiler, and K. Fluri, *IEEE Microwave Guid. Wave Lett.* **4**, 257 (1994).
- [6] G. Beni and M.A. Tenan, *J. Appl. Phys.* **52**, 6011 (1995).
- [7] D.E. Kataoka and S.M. Troian, *Nature (London)* **402**, 794 (1999).
- [8] G. Fuhr, R. Hagedorn, T. Müller, W. Benecke, and B. Wagner, *J. Microelectromech. Syst.* **1**, 141 (1992).
- [9] A.B.D. Brown, C.G. Smith, and A.R. Rennie, *Phys. Rev. E* **63**, 016305 (2001).
- [10] A. Ajdari, *Phys. Rev. E* **61**, R45 (2000).
- [11] A. Ramos, H. Morgan, N.G. Green, and A. Castellanos, *J. Colloid Interface Sci.* **217**, 420 (1999).
- [12] N.G. Green, A. Ramos, A. González, H. Morgan, and A. Castellanos, *Phys. Rev. E* **61**, 4011 (2000).
- [13] A. González, A. Ramos, N.G. Green, A. Castellanos, and H. Morgan, *Phys. Rev. E* **61**, 4019 (2000).
- [14] N.G. Green, A. Ramos, A. González, H. Morgan, and A. Castellanos, *Phys. Rev. E* **66**, 026305 (2002).
- [15] A. Ramos, H. Morgan, N.G. Green, and A. Castellanos, *J. Phys. D* **31**, 2388 (1998).
- [16] R.J. Hunter, *Zeta Potential in Colloid Science* (Academic Press, San Diego, 1981).
- [17] J. Gunning, D.Y.C. Chan, and L.R. White, *J. Colloid Interface Sci.* **170**, 522 (1995).
- [18] H.P. Schwan, *Ann. Biomed. Eng.* **20**, 269 (1992).
- [19] V.G. Levich, *Physicochemical Hydrodynamics* (Prentice-Hall, Englewood Cliffs, NJ, 1962).
- [20] H.A. Haus and J.R. Melcher *Electromagnetic Fields and Energy* (Prentice-Hall, Englewood Cliffs, NJ, 1989).
- [21] D. Beatovic, P.L. Levin, S. Sadovic, and R. Hutnak, *IEEE Trans. Electr. Insul.* **27**, 135 (1992).
- [22] P.M. Morse and H. Feshbach, *Methods of Theoretical Physics* (McGraw-Hill, New York, 1953), Chap. 10.
- [23] The net flow given by  $u_0$  tends to infinity, since we have taken the upper boundary at infinite distance from the electrodes.
- [24] N.G. Green, A. Ramos, and H. Morgan, *J. Electrostat.* **56**, 235 (2002).